Contents List available at VOLKSON PRESS

New Materials and Intelligent Manufacturing (NMIM)

DOI : http://doi.org/10.26480/icnmim.01.2018.427.430

Journal Homepage: https://topicsonchemeng.org.my/

ISBN: 978-1-948012-12-6

POROUS GRAPHENE-MANGANESE DIOXIDE NANOWIRES COMPOSITE FILM FOR HIGH VOLUMETRIC PERFORMANCE SUPERCAPACITORS

Mingxuan Han, Hao Wang, Di Yu, Lili Jiang*, Yu Zhang

Jilin Institute of Chemical Technology, Chengde Street, Jilin City, Jilin Province, China
Corresponding Author: jianglidipper@126.com

ARTICLE DETAILS

Article History:

Received 26 June 2018
Accepted 2 July 2018
Available online 1 August 2018

ABSTRACT

We report a novel strategy to prepare densely packed porous graphene and MnO_2 nanowires composite film (PGNs-MnO_2 NWs) through graphene etching process, hydrothermal method and subsequent vacuum-assisted filtration method. The ion diffusion ability of the PGNs-MnO_2 NWs film is greatly enhanced due to the contribution of cross-plane diffusion from porous graphene and in-plane diffusion from MnO_2 nanowires-graphene sandwiched structure. Based on its high surface area, fast ion diffusion and high film density, the PGNs-MnO_2 NWs film electrode exhibits high volumetric specific capacitance of 206 F cm^{-3} at 5 mV s^{-1} in 1 M Na_2SO_4 aqueous solution. The capacitance remains 99.5% after 2000 cycles of the cyclic voltammetry method. The strategy provides a facile and effective method to achieve high performance electrode materials for supercapacitor.

KEYWORDS

Porous graphene, Manganese dioxide nanowires, Composite film, Volumetric performance, Supercapacitors.

1. INTRODUCTION

As the pint-sized electrical devices are developing rapidly, subminiature energy storage facilities with excellent performances are necessary, including the energy density, the power density and the cycle life. According to study, the supercapacitors, an arresting energy storage device, have huge power density, rapid charge-discharge speed and long cycle life [1-5]. However, it is an enormous challenge that improving the energy density of supercapacitors [6,7]. In order to meet the energy demands for the practical applications in the future, supercapacitors should possess high operating voltage and high energy without immolating the power delivery or cycle life [8-11]. Moreover, the electrochemical performances of the supercapacitors were mainly decided by the electrode material. The graphene, with high surface area, eminent electrical conductivity and splendid mechanical properties, is regarded as a greatly promising electrode material for the supercapacitors. However, graphene sheets tend to form irreversible agglomerates or even restack due to their strong π–π stacking and van der Waals interactions between the entered sheets of graphene, resulting in a dramatic decrease of the effective surface area and specific capacity [12,13]. To perfect this phenomenon, it is an effective method that providing pseudocapacitances to enhance the capacitance with the metal oxide, such as NiO, MoO_3, MnO_2 and Co_3O_4. Additionally, increasing the bulk density is also a resultful strategy, which can be achieved with graphene fiber, graphene sheets and graphene film as electrode materials [14-17]. As for the graphene film, the performance of ions at its electrochemical interfaces to transport is critical [18-21]. The inserted metal oxide can prop the layers of the grapheme film to enhance the area of interfaces, which can improve the capacitance with fast ion transport [22,23].

Herein, we report the strategy to prepare the porous graphene and MnO_2 nanowires composite (PGNs-MnO_2 NWs) film. The preparation of MnO_2 NWs is a one-step hydrothermal method and the assembling of the porous graphene and MnO_2 nanowires composite film are achieved using a plain vacuum-assisted filtration method [24]. Fast ion diffusion is mainly contributed to cross-plane diffusion from porous graphene and in-plane diffusion from MnO_2 NWs-graphene sandwiched structure. The obtained PGNs-MnO_2 NWs film showed a high volumetric specific capacitance of 206 F cm^{-3} at 5 mV s^{-1} in 1 M Na_2SO_4 aqueous solution. And the capacitance remains 99.5% after 2000 cycles of the cyclic voltammetry method [25-27].

2. EXPERIMENTAL SECTION

2.1 Preparation of PGNs (porous graphene)

Firstly, 100 mL suspension of GO (0.5 mg mL^{-1}) was dispersed evenly for 1 h using ultrasonic treatment. Then, $KMnO_4$ was added into the dispersion under stirring. It was heated for 5 min with a microwave oven. Accordingly, 50 mL deionized water, 100 μL hydrazine and 350 μL ammonia were all added into the mixture above. After stirring for 10 min, it was maintained at 100 °C for 20 min with water bath. Finally, the product was washed with oxalic acid and deionized water several times to remove the impurity.

2.2 Preparation of MnO_2 NWs (MnO_2 nanowires)

To be specific, 1.75 mmol of CH_3COOK, 1 mmol of $MnSO_4{\cdot}H_2O$ and 1.75 mmol of $KClO_3$ were evenly dispersed in 15 mL deionized water. Then 0.8 mL CH_3COOH was added in the solution under stirring. The mixture above was transferred in a 25 mL stainless steel autoclave with Teflon and kept at 160 °C for 8 h. Finally, the precipitates were washed with deionized water and ethanol several times and dried at 60 °C.

2.3 Preparation of PGNs-MnO_2 NWs film

PGNs-MnO_2 NWs film was achieved using a plain vacuum-assisted filtration method. PGNs and MnO_2 NWs were measured with the mass ratio of 1:4, dispersing evenly in 300 mL deionized water using the ultrasonic bath. Then the suspension was vacuum filtrated with the mixed cellulose ester filter membrane (0.45 μm pore size). The obtained PGNs-MnO_2 NWs film was dried in the shade, and it was separated away from the filter membrane. Finally, it was transferred into a quartz tube furnace

heated to 300 °C for 2 h in N_2, and the final film was 0.5 mg cm^{-1}.

2.4 Electrochemical measurements

All the electrochemical measurements were executed in 1 M Na_2SO_4 aqueous solution utilizing a three-electrode system on a CHI 660E. The as-prepared PGNs-MnO_2 NWs films were cut into square pieces of 1×1 cm^2. And the pieces were pressed between two nickel foam with a tablet machine as the working electrode. The platinum electrode was regarded as counter and the SCE electrode as reference electrode. The gravimetric specific capacitances (C) of the three-electrode system were computed based on the CV curves at different scan rates:$C = (\int IdV)/(mvV)$.

3. RESULTS AND DISCUSSION

The PGNs-MnO_2 NWs film was successfully prepared with admirable flexibility (**Figure 1**a). As shown in **Figure 1**b, the MnO_2 was consists of chaotically overlong nanowires. These nanowires were interlaced with each other, forming a porous net structure. And the diameters of the nanowires were about 50 nm. The network could not only promote the continuous electron transfer but also provide porous structure to form more paths for ions transmission. **Figure 1**c showed that there were holes and drape structure in the PGNs surface. The huge macropores on every single layer of the graphene made it possible that irons transmitted through the layers on vertical direction. As shown in **Figure 1**d and **Figure 1**e, the MnO_2 NWs was tightly linked with the PGNs, and the average thickness of the PGNs-MnO_2 NWs film was about 4 μm. The MnO_2 NWs filled the room between graphene layers, supporting the layers of the PGNs, hindering the agglomeration of graphene layers. The porous and drape structures were obvious in **Figure 1**f. The size of these holes were about 2-5 nm. Ample porous structure played an important role in ion transportation between the graphene sheets in the cross-plane direction. Based on the unique structure, it was highly expected that PGNs-MnO_2 NWs film would exhibit a more excellent electrochemical performance.

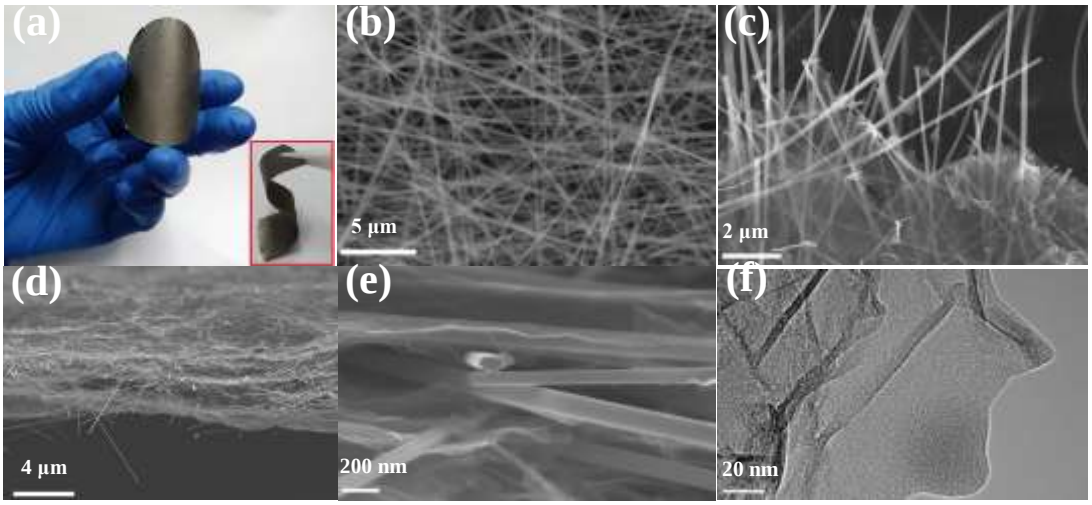

Figure 1: (a) The optical images of the PGNs-MnO_2 NWs film. (b) The SEM image of the MnO_2 NWs. (c-e) The SEM images and (f) TEM image of PGNs-MnO_2 NWs film.

The PGNs exhibited a broad XRD peak at 2θ=23° and a weak peak at 2θ=43°, corresponding to the (002) plane and the (100) plane of the graphene, respectively. (Figure 2a) The peak before 2θ=12° corresponding to micropores structure. All the peaks of the MnO_2 NWs could be regarded as α-MnO_2, which showed the same values of the standard card (PDF 81-1947). (Lan et al., 2013) Moreover, the intensity of the relative diffraction peaks of PGNs-MnO_2 NWs film was distinctly decreased compared with those of the pure MnO_2 NWs samples, which was attribute to the addition of PGNs sheets. It could be broadly seen that there were two broad peaks at 1360 cm^{-1} and 1580 cm^{-1} in both PGNs-MnO_2 NWs film and PGNs, meaning the D and G bands of graphene, respectively. (Figure 2b) In the Raman spectrum, the G band represented the in-plane bond-stretching motion of the pairs of PGNs sp^2 atoms, while the D band squared the breathing modes of rings or κ-point phonons of A_{1g} symmetry. In addition, for the PGNs-MnO_2 NWs film, there was an additional broad peak centered around 600 cm^{-1}, which may be attributed to the characteristic peak of Mn-O lattice vibrations. Raman spectroscopy further confirmed that the PGNs-MnO_2 NWs film had higher I_D/I_G ratio than the PGNs, meaning more disordered and defective carbon. It also signified the existence of more porous structure caused by the MnO_2 NW, which was agreed with the result of the SEM. The PGNs-MnO_2 NWs film indicated two main weight loss regions in air. (Figure 2c) The first region meant the evaporation of the water and the pyrolysis of oxygen containing functional groups in PGNs sheets. It was accompanied by a distinct weight loss of 10 wt % at 400 °C. The second region was the decomposed graphene while the Mn_2O_3 remained in the air atmosphere. Herein, the estimated mass percentage of the MnO_2 NWs was about 70 wt %. The PGNs exhibited a typical IV type nitrogen adsorption/desorption isotherm with an evident hysteresis loop at relative pressure P/P_0 of 0.45-0.9, (Figure 2d) meaning the existence of mesopores. With the high specific surface area of 236 m^2 g^{-1}, its total pore volume could attain 0.33 cm^3 g^{-1}. It could be well confirmed by the pore size distribution (Figure 2d insert). The insert showed that the mesopores were the main holes of the PGNs, and their size were 2-5 nm.

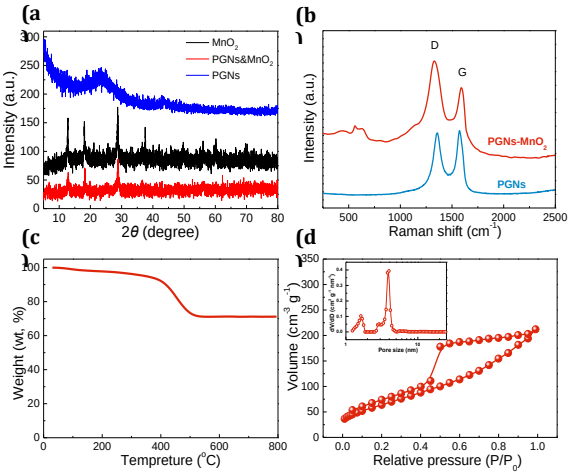

Figure 2: (a) The XRD patterns of the MnO_2 NWs, the PGNs and the PGNs-MnO_2 NWs film. (b) Raman patterns of the PGNs and the PGNs-MnO_2 NWs film. (c) The TGA curve of the PGNs-MnO_2 NWs film. (d) Nitrogen adsorption/desorption isotherms of the PGNs. The insert was the pore size distribution with the DFT method.

The electrochemical performance tests of the integral film electrode were performed in a three-electrode system using 1 M Na_2SO_4 aqueous solution. Electrochemical characterizations of the PGNs-MnO_2 NWs film (thickness of 4 μm, Figure 1d) display superior performances without the need for any other binders or electro-active additives. All the CV curves at different scan rate of the PGNs-MnO_2 NWs film exhibited rectangular-like shape from 20 mV s^{-1} to 500 mV s^{-1}, which meant admirable capacitive behaviors. (Figure 3a) It was beneficial to rapid charge transmitting with little equivalent series resistance and excellent rate performance. The galvanostatic charge/discharge profiles (Figure 3b) exhibited some highly symmetrical isosceles triangle, which could be clearly observed with all the curves at various current densities from 1 A g^{-1} to 20 A g^{-1}. It was another typical characteristic of an ideal supercapacitor electrode material, meaning an excellent electrochemical reversibility. Moreover,

the IR drop was little, even at a high current density of 20 A g^{-1}, which showed a low internal series resistance of the electrode.

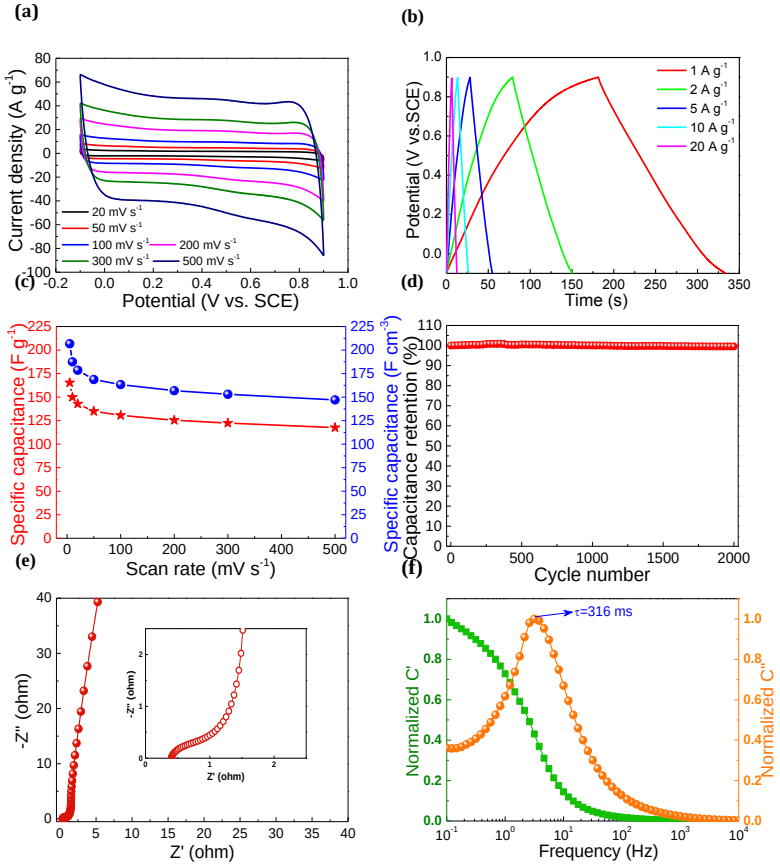

Figure 3: (a) CV curves of the PGNs-MnO_2 NWs film at different scan rates from 20 mV s^{-1} to 500 mV^{-1} (b) Galvanostatic charge–discharge curves of the PGNs-MnO_2 NWs film at different current densities. (c) The specific capacitance of the PGNs-MnO_2 NWs film at different current densities. (d) Cyclic performance of the PGNs&MnO_2 NWs film. (e) The Nyquist impedance plots of the PGNs-MnO_2 NWs film. (f) The normalized real and imaginary part capacitance of the PGNs-MnO_2 NWs film.

Figure 3c showed the specific capacitance of PGNs-MnO_2 NWs film. A high specific capacitance of 165 F g^{-1} could be observed at 5 mV s^{-1} for the PGNs-MnO_2 NWs film electrode. Correspondingly, its volumetric specific capacitance could achieve 206 F cm^{-3} at 5 mV s^{-1}. When the scan rate increased to 500 mV s^{-1}, the specific capacitance of the PGNs-MnO_2 NWs film could reach 117 F g^{-1}, which remained 70% of its initial value. The high capacitance of the PGNs-MnO_2 NWs film electrode could be ascribed to the synergistic effect of the PGNs and the MnO_2 NWs. Firstly, the MnO_2 nanowires on PGNs sheets could effectively offer the high pseudocapacitance, which increased the specific capacitance by redox reaction. Secondly, compactly connected MnO_2 nanowires could form wealthy macropores, which was beneficial for the carriage of the electrolyte ions and charge transfer reactions. Finally, the PGNs sheets in the final composite film could not only buffer the volume changing of the MnO_2 nanowires during the discharging and charging and processes, but also preserve the advanced electrical conductivity of the corporate electrode because of the excellent conductivity of PGNs. The high specific capacitance was decided by the structure of PGNs-MnO_2 NWs film. The holes and the drape provide with paths for ion transportation. Because of the high performances of the PGNs-MnO_2 NWs film, it was highly reasonable to develop an electrode material for the supercapacitors with lofty electrochemical performance. Figure 3d demonstrated the cycle life of the PGNs-MnO_2 NWs film according to CV curves. At the first 400 cycles, the PGNs-MnO_2 NWs film was unstable while it tends to be stable after the 400th cycle, even at 2000th cycle. So, the first 400 cycles could be regarded as activation. The capacitance remained 99.54%, intending excellent cycling stability.

The slant in the low frequency region suggested virtually ideal capacitive behavior. **(**Figure 3e) The interfacial contact resistance was little, which meant that connected net and whole structure could effectively reduce ion diffusion resistance. The total equivalent series resistance (ESR) was about 0.4 Ω, suggesting that the introduction of MnO_2 NWs in the layers of graphene film could enhance charge transfer depending on the connected nets and holes. Additionally, the Bode phase plots of the frequency response of capacitance (Figures 3f) also revealed the significant influence of porous structure on the rate of ion transport. The characteristic relaxation time (τ_0) of the PGNs-MnO_2 NWs film was 316 ms. Cross-plane transport was fatal for fast ion diffusion between the layers of the graphene. Excellent conductive graphene facilitated rapid electron transport, reducing the internal resistance of the electrode, which was critical for the rate capability.

4. CONCLUSION

In summary, densely packed porous graphene and MnO_2 nanowires composite film had been prepared by a simple graphene etching process hydrothermal method and subsequent vacuum-assisted filtration method. The unique structure endows fast transport of electrolyte ions and electrons throughout the film electrode due to the introduction of MnO_2 NWs in-between graphene sheets and porous graphene. As a result, the supercapacitor based on PGNs-MnO_2 NWs film electrode displays high volumetric capacitances, as well as excellent rate capability and cycling performance. Therefore, this new and simple strategy for the synthesis of the graphene-based hybrid film would open up numerous opportunities for the applications including Li-ion batteries, sensors and actuators.

ACKNOWLEDGMENTS

This work was supported by the National Natural Science Foundation of China (51702117), Major Research Projects Fund of Jilin Institute of Chemical Technology (2016006), PhD Research Startup Fund of Jilin Institute of Chemical Technology (2017002).

REFERENCES

[1] Hyun, D.Y., Gregory Salitra, E.M., Sharon, D., Aurbach, D. 2014. On the challenge of developing advanced technologies for electrochemical energy storage and conversion. Materials Today, 17, 110-121.

[2] Zhong Shuai Wu, K.P., FENG, X.L., Klaus Mu¨llen 2013. Graphene-based in-plane micro-supercapacitors with high power and energy densities. Nature Communications, 4, 2487.

[3] Li, C., Zhang, X., Wang, K., Sun, X., Liu, G., Li, J., Tian, H., Li, J., Ma, Y. 2017. Scalable Self-Propagating High-Temperature Synthesis of Graphene for Supercapacitors with Superior Power Density and Cyclic Stability. Advanced Materials, 29.

[4] Shi, X., Wu, Z.S., Qin, J., Zheng, S., Wang, S., Zhou, F., Sun, C., Bao, X. 2017.

Graphene-Based Linear Tandem Micro-Supercapacitors with Metal-Free Current Collectors and High-Voltage Output. Advanced Materials, 29.

[5] Ye, J., Tan, H., Wu, S., Ni, K., Pan, F., Liu, J., Tao, Z., Qu, Y., Ji, H., Simon, P., Zhu, Y. 2018. Direct Laser Writing of Graphene Made from Chemical Vapor Deposition for Flexible, Integratable Micro-Supercapacitors with Ultrahigh Power Output. Advanced Materials.

[6] Wang, X., Zhang, Y., Zhi, C., Wang, X., Tang, D., Xu, Y., Weng, Q., Jiang, X., Mitome, M., Golberg, D., Bando, Y. 2013. Three-dimensional strutted graphene grown by substrate-free sugar blowing for high-power-density supercapacitors. Nature Communications, 4, 2905.

[7] Meng, Y., Zhao, Y., Hu, C., Cheng, H., Hu, Y., Zhang, Z., Shi, G., Qu, L. 2013. All-Graphene Core-Sheath Microfi bers for All-Solid-State, Stretchable Fibriform Supercapacitors and Wearable Electronic Textiles. Advanced Materials, 25, 2326-31.

[8] Yu, D., Goh, K., Zhang, Q., Wei, L., Wang, H., Jiang, W., Chen, Y. 2014b. Controlled Functionalization of Carbonaceous Fibers for Asymmetric Solid-State Micro-Supercapacitors with High Volumetric Energy Density. Advanced Materials, 26, 6790-7.

[9] Ghaffari, M., Zhou, Y., Xu, H., Lin, M., Kim, T.Y., Ruoff, R.S., Zhang, Q.M. 2013. High-Volumetric Performance Aligned NanoPorous Microwave Exfoliated Graphite Oxide-based Electrochemical Capacitors. Advanced Materials, 25, 4879-85.

[10] Beidaghi, M., Gogotsi, Y. 2014. Capacitive Energy Storage in Micro-scale Devices, Recent advances in design and fabrication of microsupercapacitors. Energy and Environmental Science, 7, 867.

[11] Strauss, V., Marsh, K., Kowal, M.D., El-Kady, M., Kaner, R.B. 2018. A Simple Route to Porous Graphene from Carbon Nanodots for Supercapacitor Applications. Advanced Materials, 30.

[12] Jiang, L., Fan, Z. 2014. Design of advanced porous graphene materials: from graphene nanomesh to 3D architectures. Nanoscale, 6, 1922-45.

[13] Zhang, W., Xu, C., Ma, C., Li, G., Wang, Y., Zhang, K., Li, F., Liu, C., Cheng, H.M., Du, Y., Tang, N., Ren, W. 2017. Nitrogen-Superdoped 3D Graphene Networks for High-Performance Supercapacitors. Advanced Materials, 29.

[14] Wang, C., Xu, J., Yuen, M.F., Zhang, J., Li, Y., Chen, X., Zhang, W. 2014. Hierarchical Composite Electrodes of Nickel Oxide Nanofl ake 3D Graphene for High-Performance Pseudocapacitors. Advanced Functional Materials, 24, 6372-6380.

[15] Yu, D., Goh, K., Wang, H., Wei, L., Jiang, W., Zhang, Q., Dai, L., Chen, Y. 2014a. Scalable synthesis of hierarchically structured carbon nanotube-graphene fibres for capacitive energy storage. Nature Nanotechnology, 9, 555-62.

[16] Zheng, B., Huang, T., Kou, L., Zhao, X., Gopalsamy, K., Gao, C. 2014. Graphene fiber-based asymmetric micro-supercapacitors. Journal of Materials Chemistry A, 2, 9736-9743.

[17] Cheng, H., Dong, Z., Hu, C., Zhao, Y., Hu, Y., Qu, L., Chen, N., and Dai, L. 2013. Textile electrodes woven by carbon nanotube–graphene hybrid fibers for flexible electrochemical capacitors. Nanoscale, 5, 3428-34.

[18] Wei, L., Jiang, W., Yuan, Y., Goh, K., Yu, D., Wang, L., Chen, Y. 2015. Synthesis of free-standing carbon nanohybrid by directly growing carbon nanotubes on air-sprayed graphene oxide paper and its application in supercapacitor. Journal of Solid State Chemistry, 224, 45-51.

[19] Lausevic, Z., Apel, P.Y., Krstic, J.B., Blonskaya, I.V. 2013. Porous carbon thin films for electrochemical capacitors. Carbon, 64, 456-463.

[20] Yang, J., Zou, L. 2014. Graphene films of controllable thickness as binder-free electrodes for high performance supercapacitors. Electrochimica Acta, 130, 791-799.

[21] Yuan, C.Z., Zhou, L., Hou, L.R. 2014. Facile fabrication of self-supported three-dimensional porous reduced graphene oxide film for electrochemical capacitors. Materials Letters, 124, 253-255.

[22] Xu, H., Hu, X., Yang, H., Sun, Y., Hu, C., HUANG, Y. 2015. Flexible Asymmetric Micro-Supercapacitors Based on Bi2O3and MnO2 Nanoflowers, Larger Areal Mass Promises Higher Energy Density. Advanced Energy Materials, 5, 1401882.

[23] Cao, X., Zheng, B., Shi, W., Yang, J., Fan, Z., Luo, Z., Rui, X., Chen, B., Yan, Q., Zhang, H. 2015. Reduced graphene oxide-wrapped MoO3 composites prepared by using metal-organic frameworks as precursor for all-solid-state flexible supercapacitors. Advanced Materials, 27, 4695-701.

[24] Lan, B., Yu, L., Lin, T., Cheng, G., Sun, M., Ye, F., Sun, Q., He, J. 2013. Multifunctional free-standing membrane from the self-assembly of ultralong MnO2 nanowires. ACS Applied Materials Interfaces, 5, 7458-64.

[25] Aldaihani, N., Alenezi, R. 2017. Estimation of CO2 Emissions of the Vehicles Transport Sector in the State of Kuwait. Acta Chemica Malaysia, 1, 08-12.

[26] Singu, B.S., Yoon, K.R. 2017. Synthesis and characterization of MnO2-decorated graphene for supercapacitors. Electrochimica Acta, 231, 749-758.

[27] Zhang, N., Fu, C., Liu, D., Li, Y., Zhou, H., Kuang, Y. 2016. Three-Dimensional Pompon-like MnO2 /Graphene Hydrogel Composite for Supercapacitor. Electrochimica Acta, 210, 804-811.